# Five-Phase Induction Motor Rotor Current Observer for Finite Control Set Model Predictive Control of Stator Current

Cristina Martín, Manuel R. Arahal, *Member, IEEE*, Federico Barrero, *Senior Member, IEEE*, and Mario J. Durán

***Abstract*—Model predictive control (MPC) has recently been applied to induction motor (IM) drives in a configuration known as finite control set MPC (FCS-MPC). Its implementation must solve the problem of estimating rotor quantities, a task that is usually done using a simple backtracking procedure. On the other hand, observers have been used with field-oriented control (FOC), sensorless drives and for fault detection but they have not been used yet for finite control set predictive current control of drives. This paper shows the benefits of incorporating a rotor current observer in a finite control set model predictive controller for the stator current of a five-phase drive. The observer design methodology employed in this work uses pole placement based on Butterworth filter design. The new estimation scheme is compared with the standard one in which nonmeasurable state components and other variables are lumped into one term that is updated. The differences between both approaches are experimentally analyzed and verified.**

***Index Terms*—Finite control set, observers, pole placement, predictive control.**

## I. Introduction

MODEL predictive control (MPC) is a well established technique for process control that has been applied to electrical systems [1], later referred to as finite state MPC (FSMPC) in [2] and also finite control set MPC (FCS-MPC) in [3]. An up-to-date review of MPC applied to power electronics can be found in [4].

One implementation aspect, common to most MPC applications, is the estimation of nonmeasurable state components. These are typically rotor variables for which sensors are usually not attached. Controllers often need a good knowledge of such quantities in order to provide the best performance, being FCS-MPC a clear example. In this regard, observer theory [5] is a well-established discipline that provides a framework for understanding and designing estimation schemes for induction motor (IM) drives and other electrical systems. Its use in IM control takes either a full-order or reduced-order form. While the full-order observer makes it possible to estimate stator current and rotor components from measurements of stator voltages, stator currents, and speed [6], the reduced-order observer allows the rotor components estimation using only measurements of stator currents and speed.

Most proposals of observers for IM use the field-oriented control (FOC) scheme and related ones. However, FOC has been found in practice to be satisfactorily robust and effective without complex flux estimation methods. Otherwise, FCS-MPC is highly sensitive to prediction errors that can arise from parameter mismatch among other causes. In [7], sliding mode full-order and reduced-order observers are applied for flux and speed estimation for predictive torque control of IM. A robust model predictive current controller with a disturbance observer is also presented in [8], where a Luenberger observer is constructed for parameter mismatch and model uncertainty which affect the performance of the MPC. The gains of the disturbance observer are also determined using a root-locus analysis, and the stability of the disturbance observer is analyzed when there are errors in the inductor filter parameter. In [9], a nonlinear predictive control law with a disturbance observer is applied to track speed and flux profiles in an IM, considering the robustness to parameters' variations and the disturbance rejection. This is in contrast to most applications of FCS-MPC to electrical systems, where observers are not used as such. Instead nonmeasurable quantities, disturbances and parametric and nonparametric uncertainties are lumped into one single term of the predictive model. This term is then updated using a simple procedure and the update is hold until the next sampling period [2].

In this paper the benefits of incorporating a rotor current observer in a stator current FCS-MPC-based controller of a five-phase drive are analyzed. Research on multiphase and in five-phase IM has exploded in recent times [10]–[12], where fast control FCS-MPC-based techniques have been combined with the inherent robustness and fault tolerant characteristics of multiphase drives [13], [14].

This contribution analyzes the advantages of the proposed control scheme first using the state-space equations of the IM and later illustrating them by experimental tests. The observer design methodology employed in this paper uses pole placement based on Butterworth filter design. The new rotor quantities' estimation scheme is compared with the standard one used in FCS-MPC. The differences between both approaches are analyzed and verified with simulations and

Manuscript received May 29, 2015; revised October 28, 2015 and January 4, 2016; accepted February 3, 2016. Date of publication March 1, 2016. This work was supported in part by the Spanish Ministry of Science and Innovation under Project DPI2013-44278-R and Project ENE2014-52536-C2-1-R, in part by the Junta de Andalucía under Project P11-TEP-7555, and in part by the University of Seville, Spain (V Research Plan, action II.2).

C. Martín and F. Barrero are with the Department of Electronic Engineering, University of Seville, 41004 Seville, Spain (e-mail: cmartin15@us.es; fbarrero@us.es).

M. R. Arahal is with the Department of Systems Engineering and Automatic Control, University of Seville, 41004 Seville, Spain (e-mail: arahal@us.es).

M. J. Durán is with the Department of Electrical Engineering, University of Málaga, 29071 Málaga, Spain (e-mail: mjduran@uma.es).

Digital Object Identifier 10.1109/TIE.2016.2536578

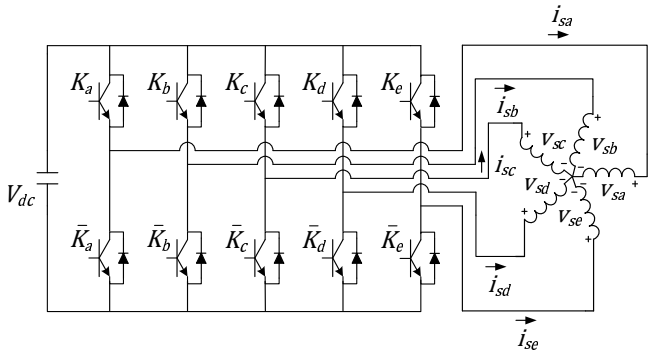


Fig. 1. Schematic diagram of the five-phase IM drive.

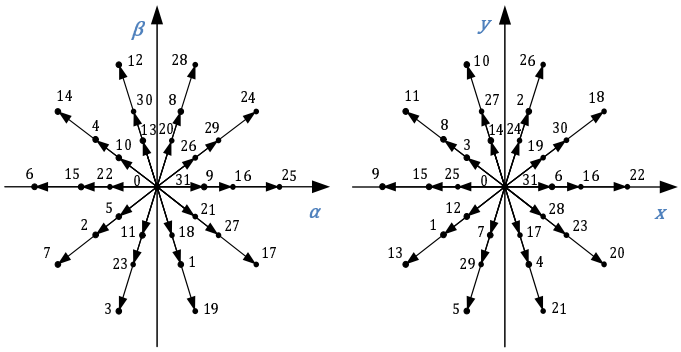


Fig. 2. Space vector diagrams in the $\alpha-\beta$ and $x-y$ subspaces.

experiments.

This paper is organized as follows. The symmetrical five-phase IM with voltage source inverter (VSI) supply used in this work is analyzed in Section II. The general principles of the FCS-MPC technique and its application to the considered system are presented in Section III. The rotor current observer is introduced in Section IV, where its design is explained and simulation results are also included to illustrate the benefits of the observer. Later, experimental results are shown and discussed in Section V, where the conventional FCS-MPC using an update and hold technique and the FCS-MPC using the Cayley-Hamilton theorem are compared with the proposed FCS-MPC methods with rotor current observer. The paper ends with conclusion section.

## II. Five-phase IM Drive Modeling

The IM drive used for testing is mainly composed of a symmetrical five-phase IM with distributed windings equally displaced $\vartheta = 2\pi/5$ and a five-phase two-level VSI. The components of the drive are schematically shown in Fig. 1 where the gating signals of the VSI are represented by $(K_a, \ldots, K_e)$.

The five-phase IM is modeled considering the standard assumptions: uniform air gap, symmetrical distributed windings, sinusoidal magnetomotive force (MMF) distribution and negligible core losses, and magnetic saturation. Then, following the vector space decomposition approach [15], the IM modeling is represented in two orthogonal subspaces. One of them is involved in the fundamental flux and the torque production ($\alpha-\beta$ subspace, representing the fundamental supply component plus supply harmonics of the order $10n\pm1$ with $n = 0, 1, 2, 3, ...$). The other is related with the losses ($x-y$ subspace, representing supply harmonics of the order $10n \pm 3$ with $n = 0, 1, 2, 3, ...$). A zero sequence harmonic component ($5n$ with $n = 1, 2, 3, ...$) is projected in the $z$-axis, but it is not considered because the neutral point is isolated. Selecting the $\alpha-\beta$ and $x-y$ stator currents and the $\alpha-\beta$ rotor currents as state variables $x_1 = i_{s\alpha}$, $x_2 = i_{s\beta}$, $x_3 = i_{sx}$, $x_4 = i_{sy}$, $x_5 = i_{r\alpha}$ and $x_6 = i_{r\beta}$, the drive equations can be cast in the form

$$\dot{x}_1 = -R_s c_2 x_1 + c_4(M\omega_r x_2 + R_r x_5 + L_r\omega_r x_6) + c_2 v_1 \quad (1)$$

$$\dot{x}_2 = -R_s c_2 x_2 + c_4(-M\omega_r x_1 - L_r\omega_r x_5 + R_r x_6) + c_2 v_2 \quad (2)$$

$$\dot{x}_3 = -R_s c_3 x_3 + c_3 v_3 \quad (3)$$

$$\dot{x}_4 = -R_s c_3 x_4 + c_3 v_4 \quad (4)$$

$$\dot{x}_5 = R_s c_4 x_1 + c_5(-M\omega_r x_2 - R_r x_5 - L_r\omega_r x_6) - c_4 v_1 \quad (5)$$

$$\dot{x}_6 = R_s c_4 x_2 + c_5(M\omega_r x_1 + L_r\omega_r x_5 - R_r x_6) - c_4 v_2 \quad (6)$$

with coefficients given by

$$c_1 = L_s L_r - M^2, \quad c_2 = \frac{L_r}{c_1}, \quad c_3 = \frac{1}{L_{ls}} \quad (7)$$

$$c_4 = \frac{M}{c_1}, \quad c_5 = \frac{L_s}{c_1} \quad (8)$$

and being the input signals the applied stator voltages $v_1 = v_{s\alpha}$, $v_2 = v_{s\beta}$, $v_3 = v_{sx}$ and $v_4 = v_{sy}$. The equations also include the rotor electrical speed $\omega_r$ and the following machine parameters, stator and rotor resistances $R_s$ and $R_r$, stator and rotor inductances $L_s$ and $L_r$, stator leakage inductance $L_{ls}$, and mutual inductance $M$.

The drive includes not only the electrical machine but also the power electronics of the VSI. And ideal inverter converts gating signals into stator voltages that can be projected to $\alpha-\beta-x-y$ axes and gathered in a row vector computed as $v = (v_{s\alpha}, v_{s\beta}, v_{sx}, v_{sy}) = V_{dc} u T M$, where $V_{dc}$ is the dc-link voltage, $u$ is a row vector containing the gating signals, $T$ is the connectivity matrix that takes into account how the VSI gating signals are distributed, and $M$ is a coordinate transformation matrix accounting for the spatial distribution of the machine windings. In the case of a five-leg inverter, the gating signals vector is defined by $u = (K_a, K_b, ..., K_e)$ were $K_j$ is the $j$th gating signal. Each gating signal can be either active $K_j = 1$ or inactive $K_j = 0$, yielding $2^5$ possible control choices and voltage vectors (see Fig. 2) at each sampling period.

Combining the above mathematical expressions a nonlinear set of equations arises, that can be written in the state-space

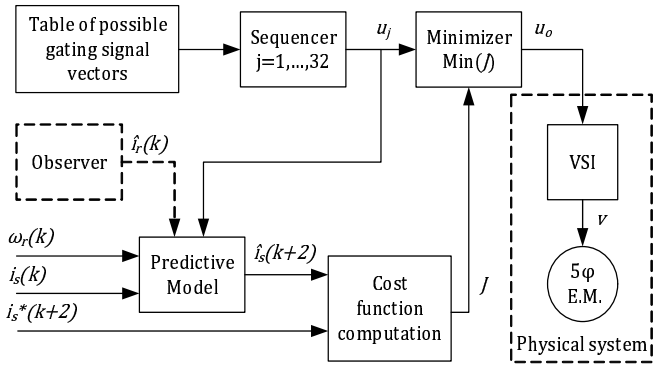


Fig. 3. FCS-MPC technique applied to a symmetrical five-phase IM drive.

form and constitutes the final drive model

$$\dot{X}(t) = AX(t) + Bv(t) \tag{9}$$

$$A = \begin{pmatrix} -a_{s2} & a_{m4} & 0 & 0 & a_{r4} & a_{l4} \\ -a_{m4} & -a_{s2} & 0 & 0 & -a_{l4} & a_{r4} \\ 0 & 0 & -a_{s3} & 0 & 0 & 0 \\ 0 & 0 & 0 & -a_{s3} & 0 & 0 \\ a_{s4} & -a_{m5} & 0 & 0 & -a_{r5} & -a_{l5} \\ a_{m5} & a_{s4} & 0 & 0 & a_{l5} & -a_{r5} \end{pmatrix} \tag{10}$$

$$B = \begin{pmatrix} c_2 & 0 & 0 & 0 \\ 0 & c_2 & 0 & 0 \\ 0 & 0 & c_3 & 0 \\ 0 & 0 & 0 & c_3 \\ -c_4 & 0 & 0 & 0 \\ 0 & -c_4 & 0 & 0 \end{pmatrix} \tag{11}$$

with state vector $X(t) = (x_1, ..., x_6)^T$ and input vector $v(t) = (v_1, ..., v_4)^T$. The coefficients of matrix $A$ are defined as $a_{s2} = R_s c_2$, $a_{s3} = R_s c_3$, $a_{s4} = R_s c_4$, $a_{r4} = R_r c_4$, $a_{r5} = R_r c_5$, $a_{l4} = L_r c_4 \omega_r$, $a_{l5} = L_r c_5 \omega_r$, $a_{m4} = M c_4 \omega_r$, and $a_{m5} = M c_5 \omega_r$.

## III. Finite Control Set Model Predictive Current Control for Drives

The FCS-MPC technique has been proposed in the literature for current control in VSI drives. The technique is illustrated by the diagram shown in Fig. 3. The objective of the controller is to track reference stator currents given by $i_s^*$. For this purpose, it uses a discrete model of the drive to predict the future behavior of the output variables $\hat{i}_s$. Then, an optimizer selects the most adequate gating signal $u_o$ to minimize a cost function $J$. The optimization is done by exhaustive search over all possible control signal values. For each one, the predictive model is computed using the measured rotor speed $\omega_r$ and stator phase currents $i_s$ to obtain the predicted values of the currents $\hat{i}_s$. Then, the cost function value is calculated and the voltage vector that minimizes the cost function is selected and applied to the VSI during the next sampling period.

The proposed FCS-MPC controller is based on [16], where a discretization technique derived from the Cayley-Hamilton equation is employed to obtain the predictive model. For simplicity, and to provide a comparison with more standard techniques, a forward Euler discretization method is also presented. It is well known that this can affect the prediction and control errors [17]. Taking this into account, the obtained predictive model from (9)-(11) yields

$$\hat{X}(k+1|k) = X(k) + T_s \left(AX(k) + Bv(k)\right) \tag{12}$$

Notice that matrix $A$ depends on the instantaneous value of the rotor electrical speed, being the predictive model a time-variant linear system. However, the mechanical dynamic is slower than the electrical one, so constant speed within a sampling period can be assumed. Consequently, matrix $A$ must be updated every sampling time using the measured $\omega_r$ and its value is held throughout the current sampling period.

The actual implementation of the FCS-MPC requires the second-step ahead prediction to be computed. This necessity arises from the fact that the computation of the control signal does take a significant amount of time which is comparable with the sampling time. In this situation, it is best to wait until the next sampling time to release the computed control signals (see [2] for details).

The final element in the FCS-MPC scheme is the cost function to be optimized. In current control, the most important figure of merit is the tracking error in predicted stator currents. For that reason, the usual cost function uses the predicted deviations from current references in the $\alpha - \beta$ and $x - y$ subspaces as

$$J = \|\hat{e}_{\alpha\beta}\|^2 + \lambda_{xy}\|\hat{e}_{xy}\|^2 \tag{13}$$

where $\hat{e}$ is the second-step ahead predicted error computed as $\hat{e} = i_s^*(k+2) - \hat{i}_s(k+2|k)$ and $\lambda_{xy}$ is a tuning parameter between 0 and 1 that allows to put more emphasis on $\alpha - \beta$ or $x - y$ subspaces. Note that a future reference value is needed, which is typically obtained from outer speed/torque loops in variable speed drives applications. However, this paper deals with current control and, for this reason, the reference is set as an input. Also, this reference is assumed to be constant in the $d - q$ reference frame and for sufficiently small sampling times, as it is indicated in [18], i.e. $i_{sdq}^*(k+2) \approx i_{sdq}^*(k+1) \approx i_{sdq}^*(k)$.

During the optimization process, both the cost function and the predictive model must be computed 32 times at each sampling period to guarantee optimality, since there are 32 possible voltage vectors for the five-phase half-bridge VSI used to drive the IM. A reduced set of voltage vectors can be, however, selected to speed up the optimization process and reduce the computational cost. In [10], a good analysis on this issue is realized, concluding that the selection of $\lambda_{xy}$ mainly depends on the number of voltage vectors to be considered.

### A. Rotor Quantities

The predictive model of (12) cannot be used in the normal operation case where rotor currents are not measured. This difficulty is usually overcome lumping all nonmeasurable terms in one factor that is later tracked and updated. As a consequence, the rotor current-related term constitutes a new variable that can be estimated using past values of the measured variables. The estimated term is projected into the future and used in the predictive model. For the case

of study, this is achieved splitting the state vector into a measurable part $X^1 = (x_1, x_2, x_3, x_4)^T$ and an unmeasurable part $X^2 = (x_5, x_6)^T$. The prediction is then obtained by simulating for a sample period the evolution of the measurable part as

$$\hat{X}^1(k+1|k) = RX^1(k) + Sv(k) + \hat{G}(k|k) \tag{14}$$

where

$$\begin{aligned} R &= (I + A_{11}T_s) \\ S &= B_1 T_s \end{aligned} \tag{15}$$

and term $\hat{G}(k|k)$ is an estimation of the contribution of $X^2(k)$ to $X^1(k+1)$. The usual estimation is obtained by holding the previous value $\hat{G}(k-1)$ computed at time $k$ as

$$\hat{G}(k-1|k) = X^1(k) - RX^1(k-1) - Sv(k-1) \tag{16}$$

To the best of our knowledge, this backtracking procedure has not been analyzed in the literature yet, and thus, the following study is novel and relevant as most proposed FCS-MPC applications rely on said procedure.

### B. Analysis of the Simple Update Method

The usual way to cope with unmeasurable (i.e., rotor) quantities in FCS-MPC is to lump them into one term that is estimated in a simple manner. The term is designated as $G$ and used in the first-step ahead prediction as

$$\hat{X}^1(k+1|k) = RX^1_m(k) + Sv(k) + \hat{G}(k) \tag{17}$$

Ideally, the term $G(k-1)$ could be computed at time $k$ by means of

$$G(k-1) = X^1(k) - RX^1(k-1) - Sv(k-1) \tag{18}$$

but, due to measurement errors $\varepsilon$, the actual estimation is

$$\hat{G}(k-1|k) = X^1_m(k) - RX^1_m(k-1) - Sv(k-1) \tag{19}$$

where $X^1_m(k)$ is the measured vector of stator quantities, linked to the real values through

$$X^1_m(k) = X^1(k) + \varepsilon(k) \tag{20}$$

Making use of the state-space equations, the estimation can be written as

$$\hat{G}(k-1|k) = \varepsilon(k) - R\varepsilon(k)(k-1) + A_{12}T_s X^2(k-1) \tag{21}$$

From this equality, it is inferred that the estimation of rotor quantities done in this way is corrupted by the measurement error. The error of the first-step ahead prediction is defined as

$$e_{1p}(k+1) \doteq X^1(k+1) - \hat{X}^1(k+1|k) \tag{22}$$

and can be computed from previous expressions as

$$\begin{aligned} e_{1p}(k+1) = {} & RX^1(k) + Sv(k) + G(k) - \\ & - \left( RX^1_m(k) + Sv(k) + \hat{G}(k-1|k) \right) \end{aligned} \tag{23}$$

It is easy to show that the above equation yields the following expression for the one-step ahead prediction error:

$$\begin{aligned} e_{1p}(k+1) = {} & -(I+R)\varepsilon(k) + R\varepsilon(k)(k-1) + \\ & + A_{12}T_s \left( X^2(k) - X^2(k-1) \right) \end{aligned} \tag{24}$$

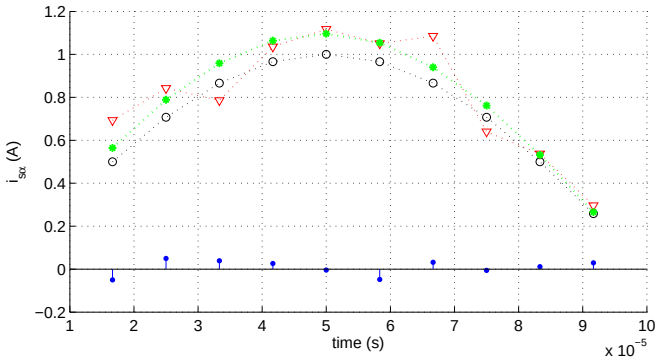


Fig. 4. Numerical example illustrating the simple method to estimate term $G$. The curve marked with circles is $i_{s\alpha}$, the real (simulated) $\alpha$ current without measurement noise. The curve marked with asterisks corresponds to an estimation using $\hat{X}^1(k+1|k) = RX^1_m(k) + Sv(k)$, i.e., without any correction for rotor quantities. The curve marked with triangles is the same estimation adding the simple update correction for $G$ given by (18), considering noise. This corresponds to the usual estimation used in FCS-MPC. The noise values are shown as filled circles and gather around their zero mean. The negative effect over the prediction is quite apparent.

From (24) one can derive that the prediction error arising from this scheme does not filter measurement errors. On average the prediction error due to this factor will exhibit the same statistical properties as $\varepsilon$. Assuming uncorrelated error measurement with a distribution with zero mean and $\sigma^2$ variance, the contribution to $e_{1p}$ variance is precisely $\sigma^2$. The instantaneous contribution can be large; for instance, if $\varepsilon(k) = -\varepsilon(k-1) = n$, then $-(I+R)\varepsilon(k) + R\varepsilon(k)(k-1) = (I+2R)n = (3I + 2A_{11}T_s)n \approx 3n$. A particular case has been simulated and illustrated in Fig. 4, where some noise in the stator current measurement has been included in the prediction process (shown as filled circles). It can be seen that a small amount of noise can produce larger deviations in the estimation of the stator current if the classical update and hold method is used.

Regarding rotor quantities, it is important to highlight that the contribution to the prediction error is filtered through the system dynamic via the term $A_{12}T_s$. For larger sampling frequencies, the effect is smaller, which is part of the reasons why most applications uses a high value of $f_s$. Also from the above expression, one can see that it is the change in rotor quantities what induces prediction error. In sinusoidal steady state, the rotor quantities are expected to evolve for the most part at the fundamental frequency $f_e$. Again, if a large $f_s/f_e$ is used, then the changes from one sampling period to the next would be small (ceteris paribus), allowing this simple estimation scheme to work. A problem might arise during transients where changes can be more pronounced.

## IV. Rotor Current Observer Design, Implementation, and Validation by Simulation

The FCS-MPC method can be modified to include an observer that estimates the nonmeasurable state components of the system. As depicted in Fig. 3, the rotor current estimation $\hat{i}_r$ is calculated by the observer using the measured rotor speed $\omega_r$ and stator phase currents $i_s$ every sampling time. This

estimation allows to use the complete state-space model (9) for predictive purposes.

It is well know from observer theory that the closed-loop poles of the observer

$$\dot{\hat{x}}(t) = A\hat{x}(t) + Bv(t) - L\left(C\hat{x}(t) - y(t)\right) \tag{25}$$

are determined by the observer gain $L$ also called Luenberger gain matrix. The error dynamic equation is simplified to

$$\dot{e}(t) = (A - LC)\, e(t) - (G - LH)\, d(t) \tag{26}$$

and the convergence toward zero is determined by the choice of the observer gain. The separation principle allows the choice of such matrix to be decoupled from the controller design.

In order to reduce the computational load required to provide estimates of all state variables of the system, a reduced-order observed can be built considering only a part of the state vector.

### A. Reduced Order Rotor Current Observer

A reduced-order observer for $i_r$ can be derived using Gopinath's method. The state is divided in two parts, the measurable one ($x^1$) and the unmeasurable part ($x^2$). In the present case, $x^1 = (x_1, x_2)^\top$ and $x^2 = (x_5, x_6)^\top$. Matrices $A$ and $B$ are accordingly divided so that

$$\begin{aligned} \dot{x}^1(t) &= A_{11}x^1(t) + A_{12}x^2(t) + B_1 v(t) \\ \dot{x}^2(t) &= A_{21}x^1(t) + A_{22}x^2(t) + B_2 v(t) \end{aligned} \tag{27}$$

The estimation for the unmeasurable part is

$$\hat{x}^2(t) = z(t) + Lx^1(t) \tag{28}$$

whose dynamic is dictated by

$$\begin{aligned} \dot{z}(t) = (A_{22} - LA_{12})\, z(t) + (A_{22} - LA_{12})\, Lx^1(t) + \\ + (A_{21} - LA_{11})\, x^1(t) + (B_2 - LB_1)\, v(t) \end{aligned} \tag{29}$$

### B. Observer Design with Butterworth Pole Placement

A correct observer design should take into account the effect of the observer gain in all terms of the error dynamic to provide a tradeoff between fast convergence and disturbance sensitivity. Ad hoc modifications of estimators suggested by observer theory often yield faster convergence without endangering stability [19]. In [20], it is noted that, 'In classical observer for IM drives, the poles of observer are designed to be proportional to the poles of IM which produces high imaginary part at high speed and is harmful to the system stability. To address this issue, it is suggested to shift the real part of observer poles to the left in the complex plane compared to the poles of IM, and the imaginary part of observer poles are not changed'. However, this leads to complicated expressions of observer gains. The authors propose a very simple constant gain matrix to improve the observer's stability.

For above reduced-order observer, the design implies the selection of the most adequate eigenvalues of $(A_{22} - LA_{12})$. As they determine the speed at which the estimation error decays, it is logical to make the real parts of those eigenvalues as negative as possible. That will force the error to decay very rapidly. However, there is a problem with this logic when there are modeling errors to be considered. In actual applications, the values in the model matrices may not be known exactly. Research has shown that in order for the observer to be robust against modeling errors, as well as causing the estimation error to decay rapidly, a different approach is required.

It is of importance that the observer has well-damped dynamic. Good damping of a system implies that the poles are located in some distance away from the origin to speed up the convergence and with imaginary parts no larger than the real parts. The latter is desirable to avoid oscillatory behavior. With poor damping, there is also a risk for instability if the observer is implemented using forward Euler discretization [19].

If the original system has $z_1$ stable zeros, then $z_1$ of the observer's eigenvalues should be placed at the values of those stable zeros. The remaining eigenvalues of the observer may be placed well into the left-half plane, but at locations that are equidistant from the origin in what is known as the Butterworth configuration. The characteristic equation from which the eigenvalues are calculated is then a Butterworth polynomial. They are a common way to specify the denominator of a low-pass filter in the area of signal processing. The step response of such filters has a slight overshoot, with good damping. The parameter $T_B$ is used to define the speed of the response, being such speed inversely proportional to $T_B$.

A second-order Butterworth filter has the characteristic polynomial

$$B(s) = T_B^2 s^2 + \sqrt{2} T_B s + 1 \tag{30}$$

By placing the poles of the observer in the location given by the roots of $B(s)$, the error dynamic has some desired characteristics with respect to damping and rise times. It is easy to see that the poles of the filter are located at

$$p = -\frac{1}{T_B\sqrt{2}} \pm j\,\frac{1}{T_B\sqrt{2}} \tag{31}$$

providing an adequate damping factor of $\zeta = \frac{1}{\sqrt{2}}$. The Luenberger gain matrix has the usual form

$$L = \begin{pmatrix} g_1 & -g_2 \\ g_2 & g_1 \end{pmatrix} \tag{32}$$

where coefficients $g_i$ are derived using the Kautsky-Nichols algorithm [21] to match the desired closed-loop observer poles. Now, as the coefficients of $A_{22}$ are dependent of $\omega_r$, it is necessary to solve the pole placement problem for the current value of $\omega_r$. In order to avoid the computing load imposed by computing the coefficients online, it is convenient to derive expressions for the elements of the gain matrix $L$ as a function of $\omega_r$ or to use a precomputed set of coefficients and interpolate. In the latter case, the resulting observer is equivalent to a gain-scheduled system and its performance depends on the schedule resolution as well as the accuracy of the measured values of $\omega_r$.

Fig. 5 shows the variation of the $L$ coefficients with $f_e$ for $T_{B1} = 0.0025$ (s), $T_{B2} = 0.0014$ (s), and $T_{B3} = 0.001$ (s). It can be seen that the variation in the coefficients' values is smooth, allowing one to rely on interpolation if a sufficiently high number of discrete samples are given.

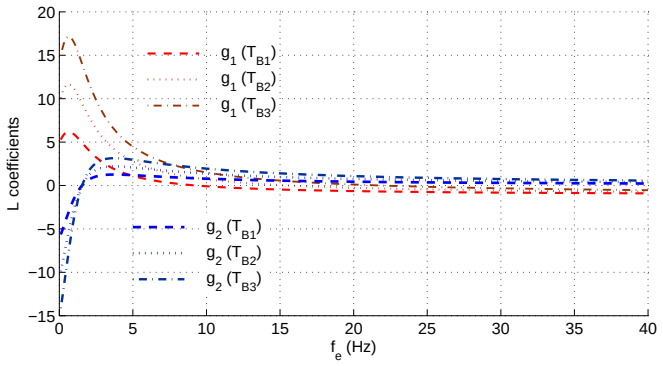


Fig. 5. Variation of $L$ coefficients versus $f_e$ for $T_{B1} = 0.0025$ (s), $T_{B2} = 0.0014$ (s) and $T_{B3} = 0.001$ (s).

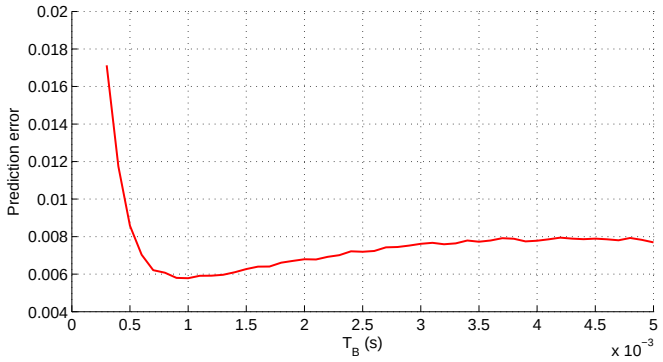


Fig. 6. Prediction error dependence on parameter $T_B$ used to tune the observer.

Fig. 6 shows the variation of the prediction error with parameter $T_B$. The errors have been obtained via extensive simulation using a model of the IM with a FCS-MPC that makes use of the observer. It can be seen that there is a global minimum at $T_B = 0.001$ (s).

### C. Simulation Results

Before showing the experimental results, the effectiveness of the proposed rotor current observer has been tested with simulations. A MATLAB simulation environment has been created for the VSI-fed symmetrical five-phase IM with distributed windings and the electrical parameters shown in Table II. Then, the conventional FCS-MPC controller and the proposed FCS-MPC controller with rotor current observer have been compared. All simulations have been carried out using a sampling time of $T_s = 67\mu$s and a stator current reference $i_s^*$ defined by the electrical frequency $f_e = 30$ Hz and the amplitude $A_{ref} = 1.20$ A. The observer has been designed using the Butterworth pole placement method commented before, with an optimum $T_B$ value of $0.001$ (s). Both predictive controllers use the 32 available voltage vectors in the optimization process. Finally, different weighting factors for the $x-y$ plane are introduced in the cost function (13) to investigate the impact of this parameter on the system performance.

Table I summarizes the obtained results, where the controllers are compared for each $\lambda_{xy}$ value on the basis of the root-mean-squared (RMS) error in the current tracking for the $\alpha$ component ($e_\alpha^{RMS}$) and for the $x-y$ plane ($e_{xy}^{RMS}$), the RMS error in the two-step ahead prediction for the $\alpha$ current component ($\hat{e}_\alpha^{RMS}$), and the total harmonic distortion in the phase currents (THD$_p$). These figures of merit are computed as follows:

TABLE I
SIMULATION RESULTS FOR $f_e = 30$ HZ AND $A_{ref} = 1.20$ A USING DIFFERENT $\lambda_{xy}$ VALUES

| $\lambda_{xy}$ | Controller | $e_\alpha^{\text{RMS}}$ (x$10^{-2}$) | $\hat{e}_\alpha^{\text{RMS}}$ (x$10^{-2}$) | $e_{xy}^{\text{RMS}}$ (x$10^{-2}$) | THD$_p$ (%) |
|---|---|---|---|---|---|
| 0.1 | FCS-MPC | 1.91 | 1.39 | 8.09 | 9.52 |
| | FCS-MPC + OBS | 1.33 | 1.38 | 7.55 | 9.06 |
| 0.5 | FCS-MPC | 2.52 | 1.38 | 4.82 | 6.05 |
| | FCS-MPC + OBS | 1.82 | 1.37 | 3.74 | 4.98 |
| 1 | FCS-MPC | 5.02 | 1.37 | 3.45 | 5.08 |
| | FCS-MPC + OBS | 2.90 | 1.36 | 2.83 | 4.49 |

$$e_\alpha^{\text{RMS}} = \sqrt{\frac{\sum_{j=1}^{N}(i_{s\alpha}(j) - i_{s\alpha}^*(j))^2}{N}} \tag{33}$$

$$e_{xy}^{\text{RMS}} = \frac{1}{2}\left(\sqrt{\frac{\sum_{j=1}^{N} i_{sx}^2(j)}{N}} + \sqrt{\frac{\sum_{j=1}^{N} i_{sy}^2(j)}{N}}\right) \tag{34}$$

$$\hat{e}_\alpha^{\text{RMS}} = \sqrt{\frac{\sum_{j=1}^{N}(\hat{i}_{s\alpha}(j+2) - i_{s\alpha}(j+2))^2}{N}} \tag{35}$$

$$\text{THD}_p = \frac{1}{5}\sum_{j=a}^{e}\sqrt{\frac{\int_0^\infty (i_{sj}(t) - i_{sj1}(t))^2 dt}{\int_0^\infty (i_{sj1}(t))^2 dt}} \tag{36}$$

where $i_{sj1}$ is the fundamental component of the considered current. THD$_p$ is obtained as the average value of the THD of all stator phase currents.

The use of the rotor current observer clearly improves the system performance in both $\alpha-\beta$ and $x-y$ subspaces for all considered $\lambda_{xy}$ values. This is confirmed by the reduction in the current tracking errors $e_\alpha^{\text{RMS}}$ and $e_{xy}^{\text{RMS}}$ (see Table I) when the observer is included in the conventional FCS-MPC controller. The achieved reduction reaches 42% for $e_\alpha^{\text{RMS}}$ and 22% for $e_{xy}^{\text{RMS}}$. Since $\alpha-\beta$ components are in relation with the electromechanical energy conversion, the improved current tracking in this plane reduces the torque ripple and enhances the dynamic performance. Additionally, the lower RMS error value in the $x-y$ plane improves the efficiency of the machine, diminishing copper losses. The harmonic content is also reduced using the rotor current observer, as evidences the lower THD$_p$ values and, consequently, stator phase current ripples. Regarding prediction errors, the FCS-MPC with rotor current observer generates lower $\hat{e}_\alpha^{\text{RMS}}$ values, as it is shown in Table I. These preliminary results are expected from observer theory [19] and must be confirmed through experimentation, where effects like measurement errors, electrical and mechanical noises or detuning of the IM modeling, among others, appear.

Notice that the use of different $\lambda_{xy}$ factors generates different control criteria and can restrict the use of voltage

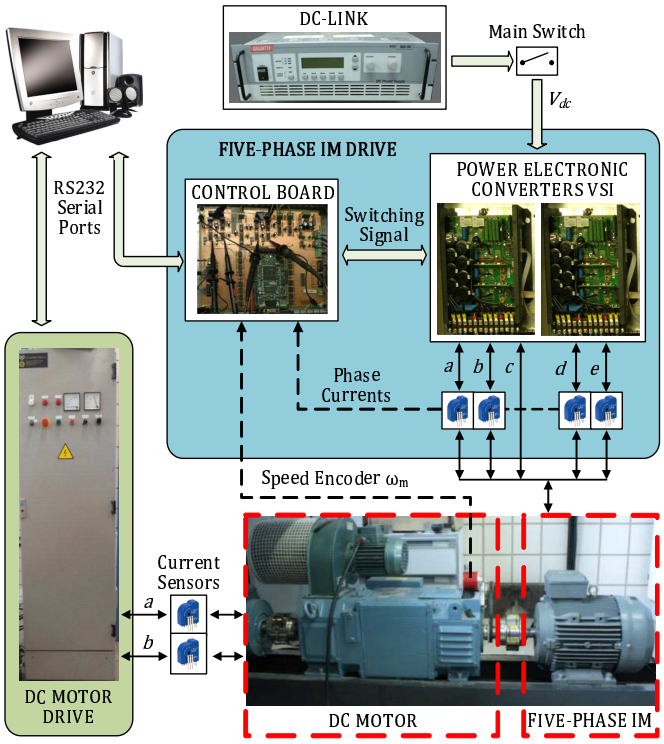


Fig. 7. Experimental apparatus diagram showing two conventional three-phase VSIs (upper right), the electronic control board (center middle), the dc motor drive (left side), the IM machine, and the dc motor (bottom right).

vectors, as it is stated in [10]. In this regard, Table I shows that the larger $\lambda_{xy}$ is, the lower $e_{xy}^{\text{RMS}}$ error is obtained for both controllers, although the RMS error in the $\alpha-\beta$ plane increases. In what follows, a low $\lambda_{xy}$ value will be mainly used to improve the torque production in the multiphase drive.

## V. Experimental Results

A laboratory experimental setup has been used for testing the proposed FCS-MPC with rotor current observer. A graphic diagram of the test rig is shown in Fig. 7. The principal element is a 30-slot symmetrical five-phase induction machine with distributed windings and three pairs of poles. The IM parameters are summarized in Table II and have been experimentally obtained using the methods described in [22] and [23]. Two SKS21F three-phase inverters from Semikron have been connected to a dc-link voltage of 300 V using an independent dc power supply. The control algorithm is deployed in a TM320F28335 digital signal processor (DSP) placed on a MSK28335 Technosoft board. A dc motor is used to introduce a variable load in the system. Finally, the rotor mechanical speed is measured using a GHM510296R/2500 digital encoder and the enhanced quadrature encoder pulse (eQEP) peripheral of the DSP.

Different tests have been carried out using four current control methods for comparison purposes: FCS-MPC technique without observer and employing the simple update and hold method for estimating the term $G$, where the effect of varying rotor quantities and perturbations are lumped (C1a in what follows), or using the Cayley-Hamilton theorem (C1b from now on); FCS-MPC with a rotor current observer used in the calculation of prediction at $(k+1)$ time (C2); and FCS-MPC with a rotor current observer used in the calculation of predictions at $(k+1)$ and $(k+2)$ times (C3). Notice that C1a controller is the one described in Section III and C1b controller is based on the predictive current control presented in [16] but using the cost function defined in (13). Also notice that both C2 and C3 controllers are introduced in the context of stator current control of IM drives and can be extended to any $n$-phase induction machine (including the three-phase one) provided that the machine has distributed windings and the torque/flux production is purely related to the $\alpha-\beta$ subspace.

TABLE II
Electrical and Nominal Parameters of the Five-Phase IM

| Parameter | | Value |
|---|---|---|
| Stator resistance | $R_s$ ($\Omega$) | 19.45 |
| Rotor resistance | $R_r$ ($\Omega$) | 6.77 |
| Stator leakage inductance | $L_{ls}$ (mH) | 100.7 |
| Rotor leakage inductance | $L_{lr}$ (mH) | 38.6 |
| Mutual inductance | $M$ (mH) | 656.5 |
| Stator rated current | $I_n(A)$ | 2.5 |
| Nominal speed | $\omega_n$ (rpm) | 1000 |
| Power | $P$ (kW) | 1 |
| Pairs of poles | $p$ | 3 |

TABLE III
Experimental Results for Different Stator Current References

| $f_e$, $A_{ref}$ (Hz, A) | Ctrl | $e_\alpha^{\text{RMS}}$ (x$10^{-2}$) | $\hat{e}_\alpha^{\text{RMS}}$ (x$10^{-2}$) | $e_{xy}^{\text{RMS}}$ (x$10^{-2}$) | THD$_{\alpha\beta}$ (%) | THD$_p$ (%) | $N_c$ (SCPC) |
|---|---|---|---|---|---|---|---|
| 29, 1.62 | C1a | 10.9 | 15.1 | 13.0 | 7.09 | 13.4 | 68.1 |
| | C1b | 8.59 | 11.1 | 11.7 | 7.05 | 12.4 | 53.1 |
| | C2 | 10.1 | 12.8 | 9.95 | 6.73 | 10.9 | 59.2 |
| | C3 | 7.84 | 10.3 | 10.1 | 6.96 | 11.1 | 56.9 |
| 34, 1.56 | C1a | 11.2 | 15.4 | 13.3 | 7.24 | 13.6 | 50.6 |
| | C1b | 8.97 | 11.4 | 11.3 | 6.95 | 12.3 | 38.2 |
| | C2 | 9.17 | 13.2 | 9.83 | 6.22 | 10.8 | 41.9 |
| | C3 | 7.82 | 10.4 | 10.9 | 6.63 | 11.7 | 39.2 |
| 39, 1.60 | C1a | 12.1 | 16.0 | 15.4 | 6.39 | 14.4 | 35.3 |
| | C1b | 8.62 | 11.0 | 12.9 | 6.30 | 12.9 | 24.3 |
| | C2 | 9.58 | 14.8 | 11.8 | 5.74 | 11.7 | 27.9 |
| | C3 | 7.82 | 10.7 | 12.8 | 5.70 | 12.8 | 25.8 |

TABLE IV
Obtained Improvement Using C3 Over C1a and C1b Controllers

| $f_e$, $A_{ref}$ | Ctrl | $e_\alpha^{\text{RMS}}$ | $\hat{e}_\alpha^{\text{RMS}}$ | $e_{xy}^{\text{RMS}}$ | THD$_{\alpha\beta}$ | THD$_p$ | $N_c$ |
|---|---|---|---|---|---|---|---|
| (Hz, A) | | Improvement percentage (%) | | | | | |
| 29, 1.62 | C1a | 28.1 | 31.6 | 22.4 | 1.92 | 16.7 | 16.5 |
| | C1b | 8.70 | 7.00 | 13.6 | 1.34 | 10.2 | −7.14 |
| 34, 1.56 | C1a | 30.4 | 32.4 | 18.2 | 8.36 | 14.5 | 22.5 |
| | C1b | 12.9 | 8.44 | 4.15 | 4.53 | 4.92 | −2.70 |
| 39, 1.60 | C1a | 35.5 | 33.3 | 16.5 | 10.9 | 11.4 | 26.8 |
| | C1b | 9.32 | 2.73 | 0.30 | 9.63 | 1.17 | −6.50 |

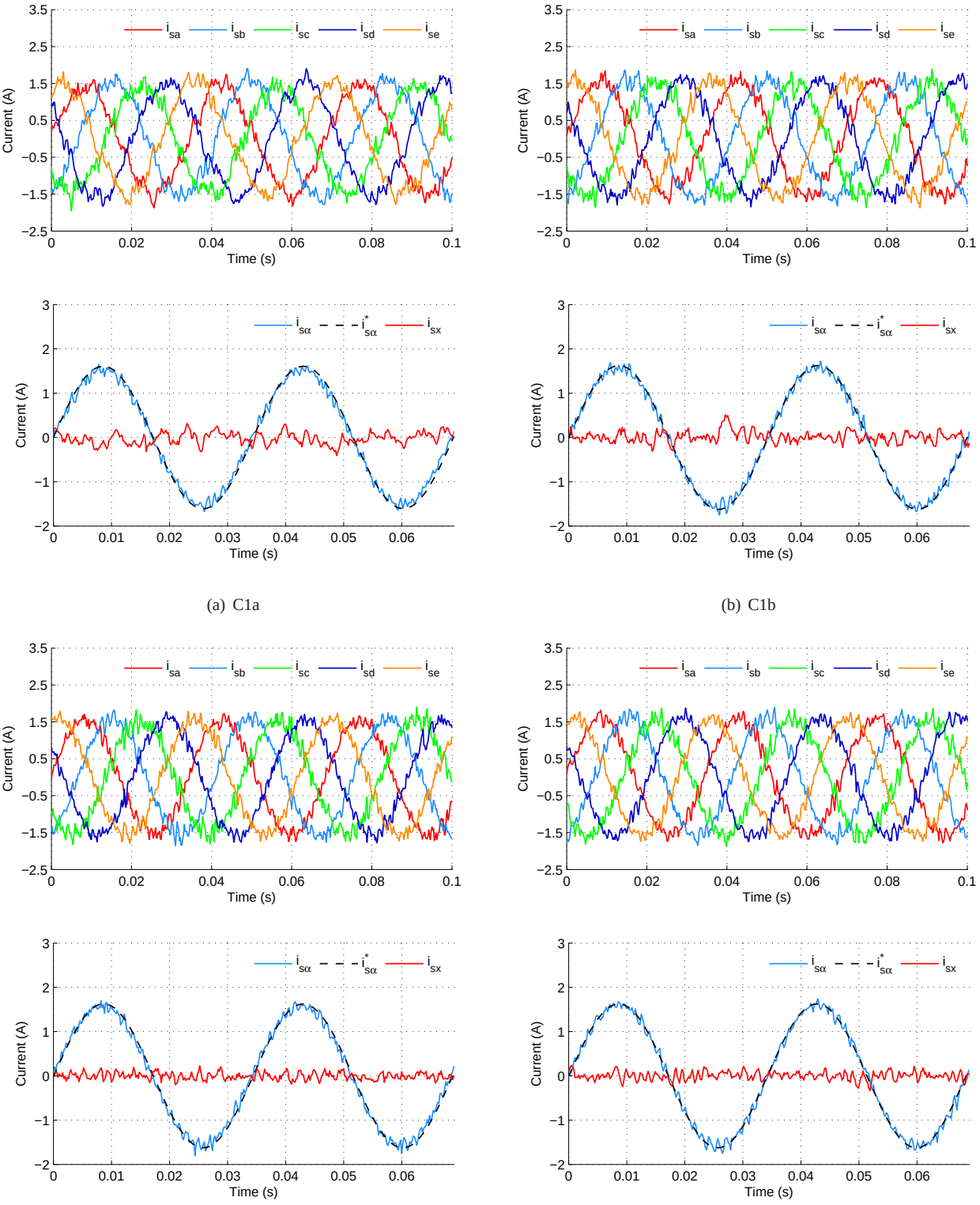


(a) C1a

(b) C1b

(c) C2

(d) C3

Fig. 8. Experimental results obtained for $A_{ref} = 1.62$ A and $f_e = 29$ Hz when it is applied the (a) C1a, (b) C1b, (c) C2, and (d) C3 controller. Upper plots show the stator phase currents $i_{sa}$, $i_{sb}$, $i_{sc}$, $i_{sd}$, and $i_{se}$, while $\alpha$ and $x$ stator currents ($i_{s\alpha}$ and $i_{sx}$) are depicted in the lower drawings.

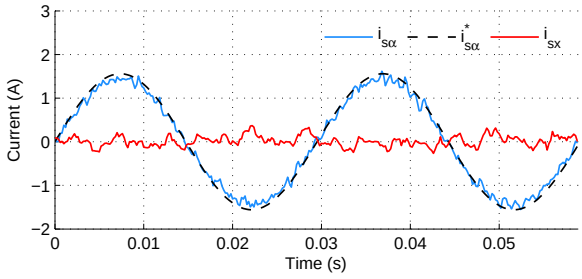


(a) C1a

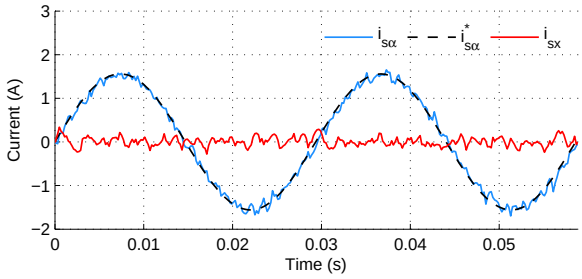


(b) C3

Fig. 9. Experimental results obtained for $A_{ref} = 1.56$ A and $f_e = 34$ Hz when it is applied the (a) C1a and (b) C3 controller. The $\alpha$ and $x$ stator currents ($i_{s\alpha}$ and $i_{sx}$) are shown.

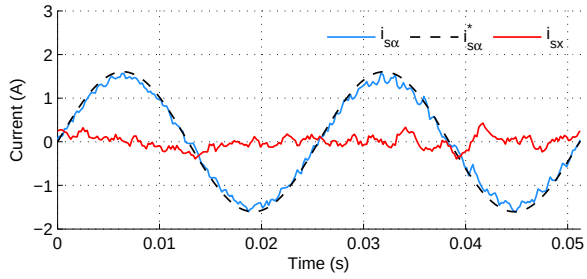


(a) C1a

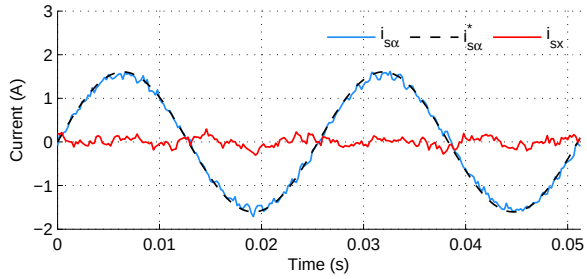


(b) C3

Fig. 10. Experimental results obtained for $A_{ref} = 1.60$ A and $f_e = 39$ Hz when it is applied the (a) C1a and (b) C3 controller. The $\alpha$ and $x$ stator currents ($i_{s\alpha}$ and $i_{sx}$) are shown.

All experiments are realized using a sampling time of $T_s = 66.67\mu$s and considering the 32 available voltage vectors, while the observer is designed using the Butterworth pole placement method (31) with $T_B = 1/1300$ (s), which is an optimum value obtained from the theoretical one (see Fig. 6) and through experimentation. The steady-state response of the system has been tested for different stator current references, where a 58% of the nominal load torque is applied and a $\lambda_{xy} = 0.1$ weighting factor is used to favor the control of the $\alpha-\beta$ plane. Table III summarizes the conditions for each test and the obtained results. The first two columns indicate the electrical frequency $f_e$ and amplitude $A_{ref}$ of the stator current reference $i^*_s$, and the applied controller (C1a, C1b, C2 and C3). The next three columns detail: the RMS error in the current tracking for the $\alpha$ component ($e^{\text{RMS}}_{\alpha}$) and for the $x-y$ components ($e^{\text{RMS}}_{xy}$), as well as the RMS error of the two-step ahead prediction in the $\alpha$ current component ($\hat{e}^{\text{RMS}}_{\alpha}$). These quantities are computed using (33)-(35), respectively. The last three columns in Table III present the THD in the $\alpha-\beta$ plane (THD$_{\alpha\beta}$), THD$_p$ and the number of switching changes per cycle ($N_c$). The $N_c$ value is obtained as the average value (over the VSI phases) of the number of switch changes per cycle (SCPC), while the THD$_{\alpha\beta}$ value is calculated similarly to (36) as follows:

$$\text{THD}_{\alpha\beta} = \frac{1}{2}\sum_{j=\alpha,\,\beta}\sqrt{\frac{\int_0^{\infty}(i_{sj}(t)-i_{sj1}(t))^2dt}{\int_0^{\infty}(i_{sj1}(t))^2dt}} \qquad (37)$$

Additionally, Table IV presents the benefits of using a rotor current observer in all figures of merit. Some of these experimental tests are graphically included to illustrate the obtained results. Fig. 8 shows the evolution of stator phase currents, and $\alpha$ and $x$ stator currents using C1a, C1b, C2 and C3 controllers in an operation point defined by $f_e = 29$ Hz and $A_{ref} = 1.62$ A. For clarity reasons, $\beta$ and $y$ stator currents have been omitted since they show similar curves. Similarly, Figs. 9 and 10 present the $\alpha$ and $x$ stator currents for C1a and C3 controllers, when the electrical frequency is set to 34 and 39 Hz, respectively. In this case, C1b and C2 controllers have not been included for simplicity reasons.

TABLE V
EXPERIMENTAL RESULTS USING DIFFERENT $\lambda_{xy}$ VALUES FOR $f_e = 29$ HZ AND $A_{ref} = 2.03$ A

| $\lambda_{xy}$ | Ctrl | $e^{\text{RMS}}_{\alpha}$ (x$10^{-2}$) | $\hat{e}^{\text{RMS}}_{\alpha}$ (x$10^{-2}$) | $e^{\text{RMS}}_{xy}$ (x$10^{-2}$) | THD$_{\alpha\beta}$ (%) | THD$_p$ (%) | $N_c$ (SCPC) |
|---|---|---|---|---|---|---|---|
| 0.1 | C1a | 11.8 | 16.3 | 12.4 | 5.28 | 9.83 | 54.3 |
| | C1b | 8.90 | 12.1 | 11.7 | 5.25 | 9.33 | 40.0 |
| | C2 | 9.89 | 15.0 | 9.99 | 4.86 | 8.35 | 46.8 |
| | C3 | 8.49 | 11.9 | 10.5 | 5.24 | 8.85 | 44.7 |
| 0.5 | C1a | 12.3 | 16.3 | 8.23 | 5.28 | 7.89 | 57.7 |
| | C1b | 9.18 | 12.1 | 8.49 | 5.34 | 7.92 | 42.2 |
| | C2 | 10.1 | 15.0 | 7.58 | 4.92 | 7.18 | 49.9 |
| | C3 | 8.91 | 11.2 | 7.27 | 5.14 | 7.10 | 47.9 |
| 1 | C1a | 15.3 | 16.5 | 7.82 | 5.64 | 8.15 | 61.1 |
| | C1b | 9.83 | 11.6 | 8.11 | 5.08 | 7.70 | 42.6 |
| | C2 | 10.6 | 15.1 | 6.85 | 5.13 | 7.02 | 52.5 |
| | C3 | 9.30 | 11.6 | 7.05 | 5.30 | 7.16 | 50.1 |

It can be stated from the obtained results that the $\alpha$ current tracking error $e^{\text{RMS}}_{\alpha}$ is reduced when a rotor current observer is included in the conventional FCS-MPC instead of the standard backtracking procedure (C1a). Additionally, this reduction is higher when the observer is applied not only to the first prediction but also to the first and second predictions (C3), obtaining an $\alpha$-tracking improvement of up to 35.5% for the considered operation points. This is stated in Fig. 8, where

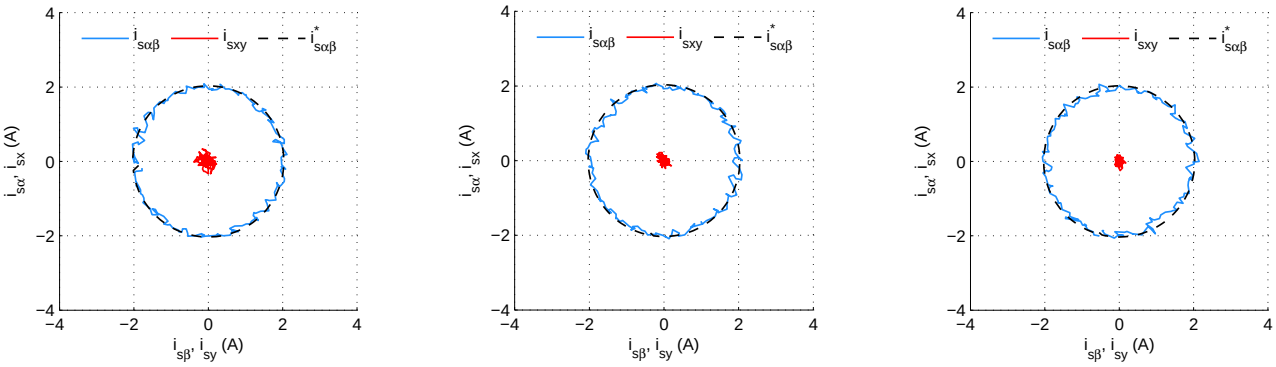


(a) $\lambda_{xy} = 0.1$ (b) $\lambda_{xy} = 0.5$ (c) $\lambda_{xy} = 1$

Fig. 11. Current trajectories in the $\alpha - \beta$ and $x - y$ subspaces with a current reference defined by $f_e = 29$ Hz and $A_{ref} = 2.03$ A. The C3 controller is used with (a) $\lambda_{xy} = 0.1$, (b) $\lambda_{xy} = 0.5$, and (c) $\lambda_{xy} = 1$.

the measured $\alpha$ current ($i_{s\alpha}$) fits better to the reference when C2 and C3 controllers are used, being C3 the best case. Note that the current tracking reduction in the $\alpha - \beta$ plane results in a lower torque ripple and, consequently, a reduction of harmonic content and losses. Also note that this $\alpha$-tracking improvement is larger with increasing frequency (see [24]), and that the use of an exact discretization technique (Cayley-Hamilton theorem C1b) can reduce the benefits of applying a rotor current observer if the estimated parameters agree with the real ones.

Moreover, the use of the rotor current observer allows to reduce considerably the RMS current tracking error in the $x-y$ subspace compared with the standard C1a controller, as it is seen in Figs. 8-10. In this issue, C2 controller has the best performance with a maximum improvement percentage in the particular figure of merit of 26%. This is an interesting benefit in multiphase machines with distributed windings, where $x-y$ components are not involved in the generation of electrical torque.

The main reason to use the rotor current observer in the conventional FCS-MPC is to produce more accurate predictions of the stator currents. Tables III and IV demonstrate this issue, where the prediction error $\hat{e}_{\alpha}^{\mathrm{RMS}}$ is reduced when C2 and C3 controllers are applied to the system. Again, C3 controller offers the best result with an improvement percentage of up to 33.3%. Similar conclusions can be obtained for the SCPC $N_c$. The use of the observer reduces up to 26.8% this figure of merit when the C3 controller is applied. It is remarkable the obtained improvement in the stator current tracking comparing with C1a when the rotor current observer is used, and this with lower VSI switching frequency. Regarding the harmonic content, its value is lower if the rotor current observer is used, being C2 the best controller in this particular figure of merit, reducing the $\mathrm{THD}_{\alpha\beta}$ and $\mathrm{THD}_p$ values 10.2% and 20.6%, respectively.

As mentioned before, the use of an exact discretization technique in the predictive model, C1b controller, improves the control performance compared with more extended C1a controllers (as it is claimed in [17]). Nevertheless, the obtained improvement using C3 remains the best, as it is shown in Table III and IV, and all considered figures of merit are reduced, except the SCPC.

TABLE VI
EXPERIMENTAL RESULTS USING DIFFERENT $T_L$ VALUES FOR $f_e = 29$ HZ

| $T_L$ (%) | Ctrl | $e_{\alpha}^{\mathrm{RMS}}$ (x$10^{-2}$) | $\hat{e}_{\alpha}^{\mathrm{RMS}}$ (x$10^{-2}$) | $e_{xy}^{\mathrm{RMS}}$ (x$10^{-2}$) | $\mathrm{THD}_{\alpha\beta}$ (%) | $\mathrm{THD}_p$ (%) | $N_c$ (SCPC) |
|---|---|---|---|---|---|---|---|
| 39 | C1a | 10.4 | 14.6 | 13.2 | 11.3 | 20.4 | 86.4 |
| | C1b | 8.70 | 10.9 | 11.5 | 10.7 | 18.3 | 68.1 |
| | C2 | 9.01 | 11.2 | 9.29 | 10.4 | 15.8 | 75.5 |
| | C3 | 8.29 | 9.83 | 9.05 | 10.7 | 15.7 | 69.5 |
| 58 | C1a | 10.9 | 15.1 | 13.0 | 7.09 | 13.4 | 68.1 |
| | C1b | 8.59 | 11.1 | 11.7 | 7.05 | 12.4 | 53.1 |
| | C2 | 10.1 | 12.8 | 9.95 | 6.73 | 10.9 | 59.2 |
| | C3 | 7.84 | 10.3 | 10.1 | 6.96 | 11.1 | 56.9 |
| 78 | C1a | 11.8 | 16.3 | 12.4 | 5.28 | 9.83 | 54.3 |
| | C1b | 8.90 | 12.1 | 11.7 | 5.25 | 9.33 | 40.0 |
| | C2 | 9.89 | 15.0 | 9.99 | 4.86 | 8.35 | 46.8 |
| | C3 | 8.49 | 11.9 | 10.5 | 5.24 | 8.85 | 44.7 |

Different experimental tests were also carried out, using the weighting factor $\lambda_{xy}$ values of 0.1, 0.5 and 1, and using a load torque equivalent to the 78% of the nominal one. The frequency and amplitude of stator current reference were configured to be $f_e = 29$ Hz and $A_{ref} = 2.03$ A, while the rest of the applied experiment's conditions were the same that those used to obtain Table III. The obtained results confirm previous ones and are summarized in Table V for each controller and figure of merit. It can be concluded that C3 method offers the best performance in terms of $\alpha - \beta$ current tracking and prediction, although C2 technique shows better performance in the $x - y$ current tracking and harmonic distortion.

Results in Table V also conclude that $\alpha$ current tracking error ($e_{\alpha}^{\mathrm{RMS}}$) increases with the weighting factor ($\lambda_{xy}$) in all the analyzed controllers, being lower this figure of merit for the C3 control technique. Furthermore, the $x - y$ current tracking error ($e_{xy}^{\mathrm{RMS}}$) is reduced when $\lambda_{xy}$ increases, while the prediction error ($\hat{e}_{\alpha}^{\mathrm{RMS}}$) remains practically constant for all values of $\lambda_{xy}$. Fig. 11 depicts the polar trajectories of the stator currents in the $\alpha-\beta$ and $x-y$ planes for the considered

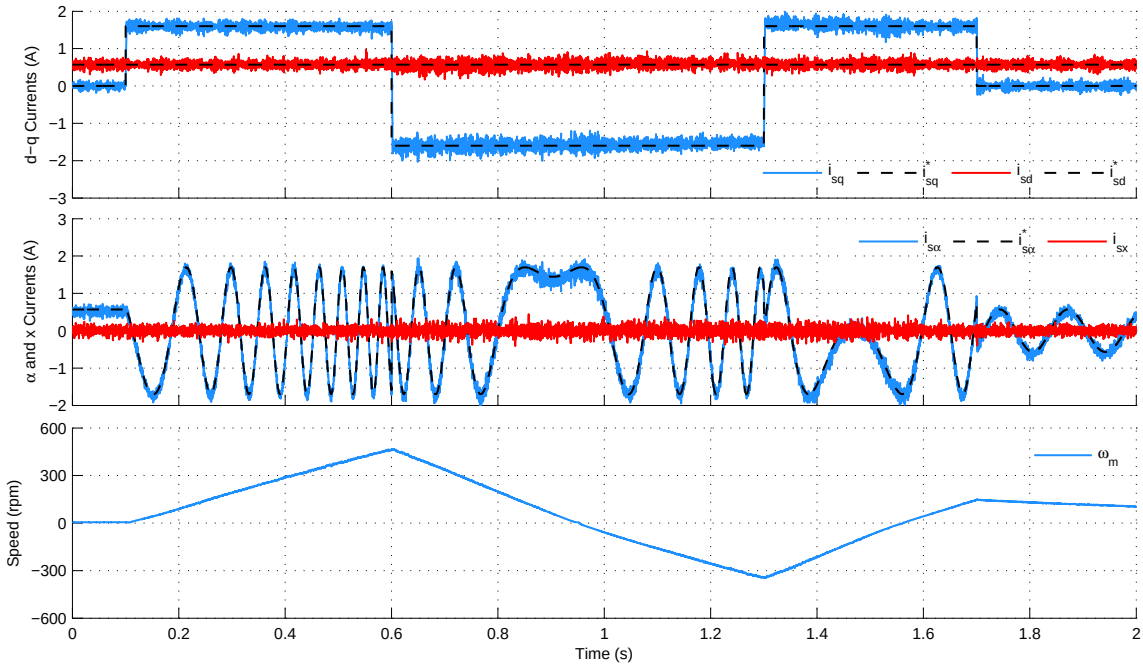


Fig. 12. Transient response using the C3 controller with stator current references $i^*_{sd} = 0.57$ A and $i^*_{sq} = 0(0,\ 0.1s)$, $1.6(0.1,\ 0.6s)$, $-1.6(0.6,\ 1.3s)$, $1.6(1.3,\ 1.7s)$ and $0(1.7,\ 2s)$. From top to bottom: $d-q$ stator currents $i_{sd}$ and $i_{sq}$, and their references $i^*_{sd}$ and $i^*_{sq}$; $\alpha$ and $x$ stator currents $i_{s\alpha}$ and $i_{sx}$, with the imposed reference $i^*_{s\alpha}$; and mechanical speed $\omega_m$.

values of $\lambda_{xy}$. Only the obtained results using C3 controller are plotted because similar curves are found using C1a, C1b and C2. It can be appreciated that $x-y$ currents decrease when $\lambda_{xy}$ value increases. On the contrary, $\alpha-\beta$ current trajectories perform worse when the weighting factor is increased.

Afterwards, some tests have been carried out varying the load torque in the multiphase drive. The experiments have been realized using a weighting factor $\lambda_{xy} = 0.1$ and an electrical frequency $f_e = 29$ Hz. Table VI resumes the obtained results for three different load toque values ($T_L$ of 39%, 58%, and 78% of the nominal one), and all considered controllers. With respect to the current tracking and prediction errors, the obtained results and conclusions remain practically the same for all load torque values. However, a reduction in the switching frequency and THD values is observed when the stator current and the load torque also increase.

Finally, a dynamic test is carried out using the C3 controller to validate the transient performance of the proposed FCS-MPC technique with a rotor current observer (similar results are obtained with C2). The dc machine does not produce load torque during the proposed test. A $\lambda_{xy}$ value of $0.1$ is used, the observer is designed with the same poles than during steady-state tests, and a total of six observer matrices are evaluated offline to take into account different rotor speeds. The $d$ stator current reference ($i^*_{sd}$) is set to $0.57$ A and the $q$ stator current reference ($i^*_{sq}$) varies in the following way: $0$ A from $0$ to $0.1$ s, $1.6$ A from $0.1$ to $0.6$ s, $-1.6$ A from $0.6$ to $1.3$ s, $1.6$ A from $1.3$ to $1.7$ s, and $0$ A from $1.7$ to $2$ s. Fig. 12 summarizes the obtained results. The measured $d-q$ stator currents ($i_{sd}$ and $i_{sq}$) fit their references well, and the step response of the $q$ current is fast. The trajectories of the $\alpha$ and $x$ currents ($i_{s\alpha}$ and $i_{sx}$) are also shown. It can be stated that the tracking performance is good even if a sudden reference change appears, displaying a rise time of about $0.002$ s. The lower plot draws the mechanical speed $\omega_m$ of the drive during the test, showing a quasi-linear response with the applied reference torque (the outer speed control loop is not used in this experiment).

Notice that from the computational cost perspective, one of the main drawbacks for the implementation of FCS-MPC in industry applications, the addition of the rotor current observer produces a negligible increment in the computational load. The total computational cost of the control algorithm with rotor current observers (C2 and C3 controllers) is estimated in $35\mu$s while it is of $32\mu$s for C1a, being $67\mu$s the sampling time.

## VI. Conclusion

Observers have been normally used in relation to several controllers: FOC, sensorless drives, and for fault detection but not, to the best of our knowledge, to estimate rotor currents in FCS-MPC techniques. In this paper, it has been shown that it is possible to incorporate a rotor current observer to the FCS-MPC to enhance the predictions, without a considerable penalty in the computational burden of the implemented controller. The obtained simulation and experimental results show that, although the simple estimate and hold scheme used by most MPC practitioners in electrical applications or the more complex MPC technique that uses the Cayley-Hamilton theorem produce acceptable results, the observer outperforms the classic approach presenting some advantages such as better current tracking performance, less harmonic content, and less VSI gating commutations. These advantages result in lower torque ripple and in higher efficiency (lower copper losses and commutations of power switches), encouraging future research

in the field where the proposed observer-based FCS-MPC can be extended to conventional and $n$-phase induction machines, just adjusting the predictive model and the observer equations to the new system.

## REFERENCES


[1] M. Lopez, J. Rodriguez, C. Silva, and M. Rivera, "Predictive torque control of a multidrive system fed by a dual indirect matrix converter," *IEEE Trans. Ind. Electron.*, vol. 62, no. 5, pp. 2731–2741, May 2015.

[2] M. Arahal, F. Barrero, S. Toral, M. Duran, and R. Gregor, "Multi-phase current control using finite-state model-predictive control," *Control Eng. Pract.*, vol. 17, no. 5, pp. 579–587, 2009.

[3] W. Xie, X. Wang, F. Wang, W. Xu, R. Kennel, D. Gerling, and R. Lorenz, "Finite control set-model predictive torque control with a deadbeat solution for PMSM drives," *IEEE Trans. Ind. Electron.*, vol. 62, no. 9, pp. 5402–5410, Sep. 2015.

[4] S. Kouro, M. A. Perez, J. Rodriguez, A. M. Llor, and H. A. Young, "Model predictive control: MPC's role in the evolution of power electronics," *IEEE Ind. Electron. Mag.*, vol. 9, no. 4, pp. 8–21, Dec. 2015.

[5] D. G. Luenberger, "An introduction to observers," *IEEE Trans. Autom. Control*, vol. AC-16, no. 6, pp. 596–602, Dec. 1971.

[6] P. L. Jansen and R. D. Lorenz, "A physically insightful approach to the design and accuracy assessment of flux observers for field oriented induction machine drives," *IEEE Trans. Ind. Appl.*, vol. 30, no. 1, pp. 101–110, Jan./Feb. 1994.

[7] S. A. Davari, D. A. Khaburi, F. Wang, and R. M. Kennel, "Using full order and reduced order observers for robust sensorless predictive torque control of induction motors," *IEEE Trans. Power Electron.*, vol. 27, no. 7, pp. 3424–3433, Jul. 2012.

[8] C. Xia, M. Wang, Z. Song, and T. Liu, "Robust model predictive current control of three-phase voltage source PWM rectifier with online disturbance observation," *IEEE Trans. Ind. Informat.*, vol. 8, no. 3, pp. 459–471, Aug. 2012.

[9] A. Merabet, M. Ouhrouche, and R.-T. Bui, "Nonlinear predictive control with disturbance observer for induction motor drive," in *Proc. IEEE Int. Symp. Ind. Electron. (ISIE)*, 2006, pp. 86–91.

[10] C. S. Lim, E. Levi, M. Jones, N. A. Rahim, and W. P. Hew, "FCS-MPC-based current control of a five-phase induction motor and its comparison with PI-PWM control," *IEEE Trans. Ind. Electron.*, vol. 61, no. 1, pp. 149–163, Jan. 2014.

[11] F. Barrero and M. J. Duran, "Recent advances in the design, modeling and control of multiphase machines-Part 1," *IEEE Trans. Ind. Electron.*, vol. 63, no. 1, pp. 449–458, Jan. 2016.

[12] M. J. Duran and F. Barrero, "Recent advances in the design, modeling and control of multiphase machines-Part 2," *IEEE Trans. Ind. Electron.*, vol. 63, no. 1, pp. 459–468, Jan. 2016.

[13] R. S. Arashloo, M. Salehifar, L. Romeral, and V. Sala, "A robust predictive current controller for healthy and open-circuit faulty conditions of five-phase BLDC drives applicable for wind generators and electric vehicles," *Energy Convers. Manage.*, vol. 92, pp. 437–447, 2015.

[14] C. Martín, M. R. Arahal, F. Barrero, and M. J. Duran, "Multiphase rotor current observers for current predictive control: A five-phase case study," *Control Eng. Pract.*, vol. 49, pp. 101–111, 2016.

[15] E. Levi, R. Bojoi, F. Profumo, H. Toliyat, and S. Williamson, "Multiphase induction motor drives-A technology status review," *IET Elect. Power Appl.*, vol. 1, no. 4, pp. 489–516, 2007.

[16] M. J. Duran, J. A. Riveros, F. Barrero, H. Guzman, and J. Prieto, "Reduction of common-mode voltage in five-phase induction motor drives using predictive control techniques," *IEEE Trans. Ind. Appl.*, vol. 48, no. 6, pp. 2059–2067, Nov./Dec. 2012.

[17] H. Miranda, P. Cortes, J. I. Yuz, and J. Rodriguez, "Predictive torque control of induction machines based on state-space models," *IEEE Trans. Ind. Electron.*, vol. 56, no. 6, pp. 1916–1924, Jun. 2009.

[18] S. Kouro, P. Cortes, R. Vargas, U. Ammann, and J. Rodriguez, "Model predictive control-A simple and powerful method to control power converters," *IEEE Trans. Ind. Electron.*, vol. 56, no. 6, pp. 1826–1838, Jun. 2009.

[19] G. C. Verghese and S. R. Sanders, "Observers for flux estimation in induction machines," *IEEE Trans. Ind. Electron.*, vol. IE-35, no. 1, pp. 85–94, Feb. 1988.

[20] Y. Zhang and H. Yang, "Model predictive torque control of induction motor drives with optimal duty cycle control," *IEEE Trans. Power Electron.*, vol. 29, no. 12, pp. 6593–6603, Dec. 2014.

[21] J. Kautsky, N. K. Nichols, and P. Van Dooren, "Robust pole assignment in linear state feedback," *Int. J. Control*, vol. 41, no. 5, pp. 1129–1155, 1985.

[22] A. G. Yepes, J. A. Riveros, J. Doval-Gandoy, F. Barrero, O. Lopez, B. Bogado, M. Jones, and E. Levi, "Parameter identification of multiphase induction machines with distributed windings-Part 1: Sinusoidal excitation methods," *IEEE Trans. Energy Convers.*, vol. 27, no. 4, pp. 1056–1066, Dec. 2012.

[23] J. A. Riveros, A. G. Yepes, F. Barrero, J. Doval-Gandoy, B. Bogado, O. Lopez, M. Jones, and E. Levi, "Parameter identification of multiphase induction machines with distributed windings-Part 2: Time-domain techniques," *IEEE Trans. Energy Convers.*, vol. 27, no. 4, pp. 1067–1077, Dec. 2012.

[24] W. S. Levine, *The control handbook*. Boca Raton, FL, USA: CRC Press, 1996.


**Cristina Martín** was born in Seville, Spain, in 1989. She received the Industrial Engineer degree from the University of Málaga, Málaga, Spain, in 2014. She has been working toward the Ph.D. degree in electronic engineering in the Department of Electronic Engineering, University of Seville, Seville, Spain, since 2015.

Her research interests include modeling and control of multiphase drives, microprocessor and DSP device systems, and electrical vehicles.

**Manuel R. Arahal** (M'06) was born in Seville, Spain, in 1966. He received the M.Sc. and Ph.D. degrees in industrial engineering from the University of Seville, Seville, Spain, in 1991 and 1996, respectively.

He is currently a Professor with the Department of Systems Engineering and Automation, University of Seville.

Dr. Arahal was the recipient of Best Paper Awards from the IEEE Transactions on Industrial Electronics for 2009, and from the IET Electric Power Applications for 2010-2011.

**Federico Barrero** (M'04–SM'05) received the M.Sc. and Ph.D. degrees in electrical and electronic engineering from the University of Seville, Seville, Spain, in 1992 and 1998, respectively.

In 1992, he joined the Department of Electronic Engineering, University of Seville, where he is currently an Associate Professor.

Dr. Barrero was the recipient of Best Paper Awards from the IEEE Transactions on Industrial Electronics for 2009 and from the IET Electric Power Applications for 2010-2011.

**Mario J. Durán** was born in Málaga, Spain, in 1975. He received the M.Sc. and Ph.D. degrees in electrical engineering from the University of Málaga, Málaga, Spain, in 1999 and 2003, respectively.

He is currently an Associate Professor with the Department of Electrical Engineering, University of Málaga. His research interests include modeling and control of multiphase drives and renewable energies conversion systems.